ACS APPLIED MATERIALS & INTERFACES

Research Article

www.acsami.org

Quantitative Determination of Ligand Densities on Nanomaterials by X-ray Photoelectron Spectroscopy

Marco D. Torelli,[†] Rebecca A. Putans,[†,§] Yizheng Tan,[†,∥] Samuel E. Lohse,[‡,⊥] Catherine J. Murphy,[‡] and Robert J. Hamers*[,†]

[†]Department of Chemistry, University of Wisconsin-Madison, 1001 University Avenue, Madison, Wisconsin 53706, United States

[‡]Department of Chemistry, University of Illinois, 600 South Mathews Avenue, Urbana, Illinois 61801, United States

Supporting Information

ABSTRACT: X-ray photoelectron spectroscopy (XPS) is a nearly universal method for quantitative characterization of both organic and inorganic layers on surfaces. When applied to nanoparticles, the analysis is complicated by the strong curvature of the surface and by the fact that the electron attenuation length can be comparable to the diameter of the nanoparticles, making it necessary to explicitly include the shape of the nanoparticle to achieve quantitative analysis. We describe a combined experimental and computational analysis of XPS data for molecular ligands on gold nanoparticles. The analysis includes scattering in both Au core and organic shells and is valid even for nanoparticles having diameters comparable to the electron attenuation length (EAL). To test this model, we show experimentally how varying particle diameter from 1.3 to 6.3 nm leads to a change in the measured A_C/A_{Au} peak area ratio, changing by a factor of 15. By analyzing the data in a simple computational model, we demonstrate that ligand densities can be obtained, and, moreover, that the actual ligand densities for these nanoparticles are a constant value of 3.9 ± 0.2 molecules nm^{-2}. This model can be easily extended to a wide range of core−shell nanoparticles, providing a simple pathway to extend XPS quantitative analysis to a broader range of nanomaterials.

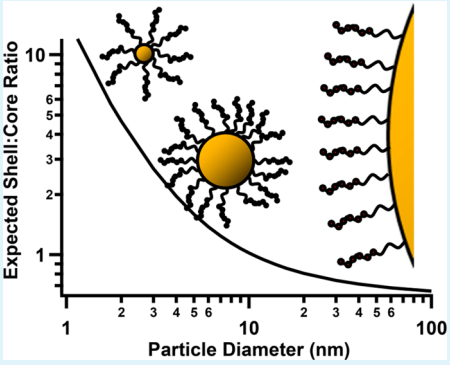

KEYWORDS: *quantitative XPS, nanoparticle, ligand density, molecular coverage*

INTRODUCTION

Organic ligands play a key role in controlling stability and other properties of many kinds of nanoparticles, as well as guiding their interactions in aqueous matrixes and in the environment. Yet, determination of ligand coverage, a key parameter, remains challenging.[1,2] Prior studies have used a number of methods to determine ligand densities including Mie scattering,[3] thermogravimetric analysis,[4] heteronuclear nuclear magnetic resonance,[5] inductively coupled plasma mass spectroscopy,[6,7] fluorescence,[8] and X-ray photoelectron spectroscopy (XPS).[9] Among these, XPS is unique in its ability to be applied to nearly any kind of nanoparticle−ligand combination; this universality is a primary reason for its widespread use characterizing organic monolayers on planar surfaces.[10−20] In XPS studies of monolayers, the bulk substrate typically acts as an internal standard, and from a knowledge of the intensity of chemical species unique to the surface and bulk, an absolute coverage can be easily obtained.[21,22] However, when applied to nanoparticles, analysis of XPS data is complicated by the fact that the curvature of the particles alters the effective number of surface and core atoms physically sampled by the instrument, leading to geometric effects that must be taken into account.[23−27] These effects are particularly important when the nanoparticle diameter is comparable to the electron inelastic mean free path (IMFP).[25,26] Early work by Frydman and co-workers analyzed emission from spherical particles of different diameters and derived an analytic integral expression for the emission from a single particle with a thin (nonscattering) shell.[26] Yet, most experimental studies[3,6,9,23−25,28−31] have used simplified approaches[3,6,9,23−25,28−31] that neglect the possibility of shell electrons traversing through the entire nanocrystal. These simplified approaches are applicable to nanoparticles with diameters that are large as compared to the IMFP (which is ∼2 nm under conditions of most XPS experiments) but fail for smaller nanoparticles.[25,26,32]

Here, we describe a combined experimental and computational study of the XPS spectra of core−shell nanoparticles that explicitly includes scattering in both core and shells, and that is valid for nanoparticles having diameters comparable to the electron attenuation length (EAL). We show how varying particle size directly changes predicted shell/core ratios and compare them to experimental results to obtain meaningful densities of organic ligands. Our results show that large variations in changes in XPS peak intensities can be accurately modeled to yield quantitative ligand densities that are

Received: October 21, 2014
Accepted: December 16, 2014
Published: December 16, 2014

DOI: 10.1021/am507300x
ACS Appl. Mater. Interfaces 2015, 7, 1720−1725

independent of particle size and in good agreement with values reported on planar surfaces.

METHODS

Functionalized gold nanoparticles with different diameters and capping ligands were synthesized using previously published methods. Detailed procedures are described in the Supporting Information. During synthesis, the nanoparticle diameter was estimated from the wavelength of the peak in the plasmon absorption band; after synthesis, the actual size distributions were measured using transmission electron microscopy. For TEM analysis, the particles were diluted 10-fold in ethanol, dried onto a 300 mesh pure carbon grid (Ted Pella), and viewed with a Philips FEG CM200 Ultra Twin TEM at 200 kV accelerating voltage. Images and size distributions are shown in the Supporting Information.

After the nanoparticles were drop-casted onto planar Si substrates, X-ray photoelectron spectra were obtained using a custom-built, ultrahigh-vacuum Phi XPS system with a base pressure of $<2 \times 10^{-10}$ Torr. X-rays were provided by an Al Kα source with a quartz-crystal monochromator. Typical measurements used pass energies of 47 eV (yielding analyzer resolution of 0.64 eV). An electron collection angle of 45° with respect to the surface normal was used for all measurements.

RESULTS

Gold Nanoparticle XPS Data. To evaluate the application of the simulation method to nanoparticles of different types, XPS spectra were obtained of Au nanoparticles with diameters of 1.3 ± 0.3, 2.1 ± 0.6, and 4.1 ± 1.3 nm that were functionalized with HS−$(CH_2)_{11}$−$(EG)_6$−COOH ligands (see the Supporting Information for more detail). XPS spectra were also obtained of Au nanoparticles with diameters of 6.1 ± 1. and 18 ± 6 nm with HS−$(CH_2)_{11}$−$(EG)_6$−OH ligands. As a reference point, we also acquired XPS spectra of a planar metal film functionalized with HS$(CH_2)_{11}$−$(EG)_6$−OH. Here, "EG" refers to the ethylene glycol group, −OCH_2CH_2−.

Figure 1 shows representative spectra of HS−$(CH_2)_{11}$−$(EG)_6$−OH-modified samples: one sample of a planar gold film and the other consisting of a film of 6.1 nm gold nanoparticles functionalized with HS−$(CH_2)_{11}$−$(EG)_6$−OH, extensively cleaned, and then made into a nanoparticle film by drop-casting. The two spectra shown here were obtained under identical experimental alignment geometries; thus, the absolute intensities can be directly compared. The data in Figure 1 show that for the nanoparticle film, the Au(4f) signal is substantially lower than that of the planar film. In the C(1s) region of the spectra, the peak at 284.7 eV is attributed to the alkyl portion of the ligand, while the peak at 286.7 eV arises from C atoms within the ethylene glycol region of the ligand.[33,34] Detailed curve-fitting (not shown) reveals an additional contribution at 287.8 eV from the carbon within the carboxylic acid for HS−$(CH_2)_{11}$−$(EG)_6$−COOH-functionalized particles.[30] Similar experiments were performed with Au nanoparticles with several different diameters and with two different ligands. The areas of the Au(4f) and C(1s) regions were determined, and atomic sensitivity factors specific for our electron energy analyzer were applied to get peak corrected area ratios A_C/A_{Au}.

Table 1 summarizes data from experimental measurements of several different sizes and with two slightly different ligands, along with the results of numerical modeling described below. Comparing HS−$(CH_2)_{11}$−$(EG)_6$−OH-functionalized samples of planar gold and gold nanoparticles, the data show that the peak area ratio A_C/A_{Au} measured on the 1.3 nm diameter Au NPs (143.8) is nearly 80 times the value (1.86) measured on

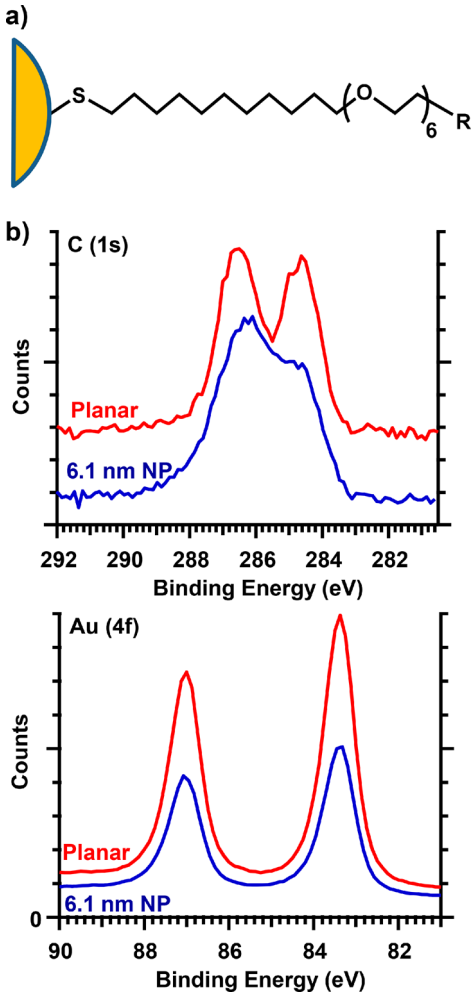

Figure 1. (a) Au nanoparticle functionalized with HS−$(C_{11}H_{22})$−$(EG)_6$−R where EG = −OCH_2CH_2−, and R = OH or R = COOH. (b) XPS spectra showing Au (4f) and C (1s) regions of planar gold and 6.1 nm gold nanoparticle samples, both functionalized with HS−$(C_{11}H_{22})$−$(EG)_6$−OH.

the planar film. While this large difference could be interpreted as an indication that the nanoparticles have a higher coverage as compared to the planar film, our analysis below shows that this difference is almost entirely due to the high curvature of the nanoparticles.

Modeling of XPS Data. Previous studies have used a simple spherical model to simulate the spectra of core−shell nanoparticles.[6,9,24,31] As typically implemented, spherical models neglect electrons emitted from the shell that traverse the entire NP before escaping.[31] This "back-side" contribution is important for very small NPs and for cores that scatter only weakly.[26] We therefore developed our model to properly include all contributions to the total observed signal. For convenience, we model the system in cylindrical coordinates, with the axis corresponding to the line-of-sight between the nanoparticle and the detection system (i.e., the electron energy analyzer in the "Z" direction). Figure 2 shows a cross-sectional view through the center of the cylinder, revealing a two-dimensional array in which each grid unit at position (r, z) is defined in terms of discrete distances $M\Delta r$ and $N\Delta z$, respectively. Each grid unit at location (M,N) is assigned to a specific material (gold, carbon, vacuum, etc.) to correspond with the physical dimensions of the particle that determine its

DOI: 10.1021/am507300x
ACS Appl. Mater. Interfaces 2015, 7, 1720−1725

Table 1. Sensitivity Corrected C/Au Ratios Measured for Various Particle Types and Final Calculated Ligand Densities Using the Numerical Modeling Approach Described Below[a]

material and ligand	A_C/A_{Au}	ligand area density, molecules nm^{-2}, and estimated error limits
planar Au + $HS(CH_2)_{11}$–$(EG)_6$–OH	2.18 ± 0.12	3.2 (3.1–3.3)
18 ± 6 nm Au + $HS(CH_2)_{11}$–$(EG)_6$–OH	2.37 ± 0.30	2.6 (2.3–2.8)
6.1 ± 1.5 nm Au + $HS(CH_2)_{11}$–$(EG)_6$–OH	8.95 ± 1.10	3.7 (3.5–3.9)
4.1 ± 1.3 nm Au + $HS(CH_2)_{11}$–$(EG)_6$–COOH	16.3 ± 2.2	3.8 (3.6–4.0)
2.1 ± 0.6 nm Au + $HS(CH_2)_{11}$–$(EG)_6$–COOH	67.2 ± 6.9	4.2 (4.0–4.4)
1.3 ± 0.3 nm Au + $HS(CH_2)_{11}$–$(EG)_6$–COOH	143.8 ± 63.1	3.8 (3.1–4.3)

[a]Also shown are the minimum and maximum error limits based on the uncertainty in the XPS data.

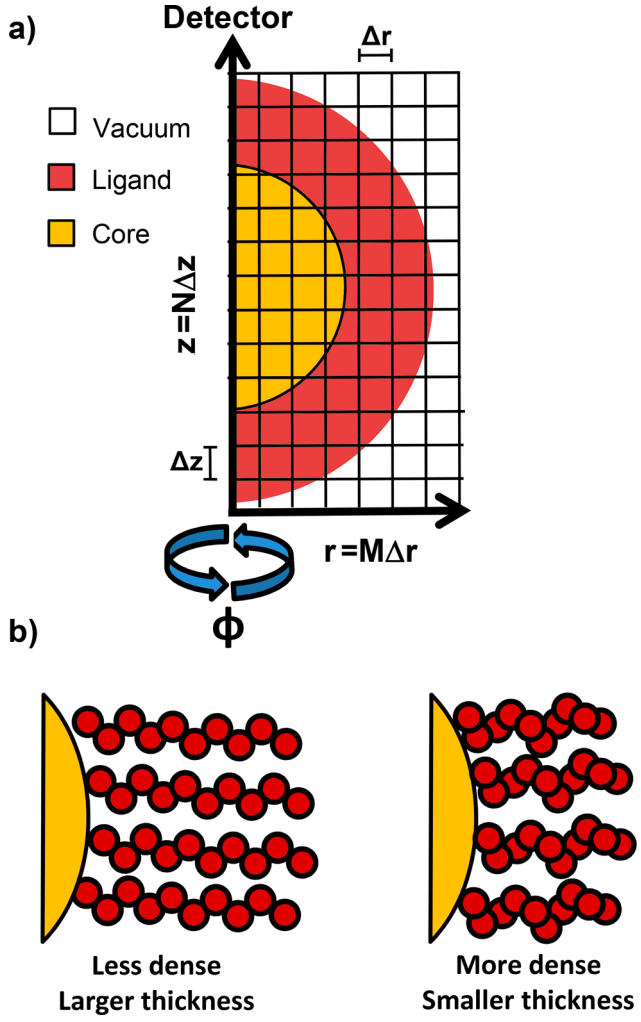

Figure 2. (a) Two-dimensional cross-section of nanoparticle model. (b) Comparison of two molecular layers with identical areal densities, but differing in the degree of compression of the monolayer. The products of volumetric density and thickness, which together determine scattering efficiency and photoelectron creation, are identical for these two cases.

role in creating electrons at a particular energy, as well as its scattering properties. The detected signal for each element is defined as the total signal measured along the positive Z direction. To arrive at the summed signal, each grid unit is iteratively summed in the Z direction, with the signal at the location (M,N) given by expression 1.

$$I_{Au(M,N)} = I_{Au(M,N-1)}\, e^{-\Delta z/\lambda_{Au,Au}} + \Delta I_{Au} \quad (1)$$

In this equation, $I_{Au(M,N)}$ is the intensity of Au electrons at a particular radius ($r = M\Delta r$) from the axis, and vertical position ($z = N\Delta z$). $I_{Au(M,N-1)}$ is the intensity of electrons leaving grid member $(M,N-1)$ and entering grid member (M,N). Within grid member (M,N), these electrons are scattered by a small amount corresponding to the thickness of the element (Δz) and the appropriate EAL for electrons of the proper kinetic energy in the given materials ($\lambda_{KE,material}$), thus reduced by an amount $e^{-\Delta z/\lambda_{Au,Au}}$, $e^{-\Delta z/\lambda_{Au,C}}$, $e^{-\Delta z/\lambda_{C,C}}$, or $e^{-\Delta z/\lambda_{C,Au}}$ corresponding to the EAL for electrons scattering in the different materials. Here, we assume that the elastic scattering is negligible, so the EAL is equivalent to the IMFP. Values used for electron scattering were of Au(4f) photoelectrons in gold ($\lambda_{Au,Au}$ = 1.63 nm),[35] Au(4f) photoelectrons in carbon ($\lambda_{Au,C}$ = 4.2 nm),[36] C(1s) photoelectrons in carbon ($\lambda_{C,C}$ = 3.8 nm), or C(1s) photoelectrons in gold ($\lambda_{C,Au}$ = 1.46 nm). Values of $\lambda_{C,C}$ and $\lambda_{C,Au}$ were obtained from the known values of $\lambda_{Au,C}$ and $\lambda_{Au,Au}$, respectively, and using the modified Wagner relation (2) for hydrocarbons to correct for a small change in escape depth with energy.[36,37]

$$\lambda_{KE_2,e_1} = \lambda_{KE_1,e_1}\cdot\left(\frac{KE_2}{KE_1}\right)^{0.67} \quad (2)$$

The grid member (M,N) itself is also a source of electrons, adding to the intensity propagating along the Z direction by an amount ΔI_{Au}. Starting at the origin, this process is iterated for each grid member N, effectively integrating the scattering of electrons as they propagate through a nanoparticle. This process is then repeated for each radius $r = M\Delta r$, using a volume element in cylindrical coordinates, $dV = dr\, d\phi\, dz$. The net result is a final intensity of electrons emitted from the core and organic layer (or other shell) along the Z direction. Such a model can be expanded to include multiple shells as needed. Instead of explicitly modeling the complete sphere as a three-dimensional matrix, the calculation can be speeded up by noting that the system has cylindrical symmetry about the Z axis. Consequently, the nanoparticle is represented internally as a planar semicircle, and the numerical values at each radius are multiplied by $2\pi r$, thereby generating the spherical nanoparticle as a volume of revolution about the Z axis.

In this model, the organic monolayer is treated as a homogeneous shell of an assumed volumetric density and unknown thickness. The calculation is run to give predicted XPS emission yields ($A_{shell}/A_{Core} = A_C/A_{Au}$) for different organic layer thicknesses. The calculated thickness that yields best agreement between experimental and calculated values of A_C/A_{Au} is then used as the effective thickness of an equivalent homogeneous layer, and the product of the density and thickness yields a number density of C atoms (atoms nm^{-2}).

DOI: 10.1021/am507300x
ACS Appl. Mater. Interfaces 2015, 7, 1720–1725

This can be divided by the number of C atoms per molecule to convert to a molecular coverage.

It is essential to note that while the calculation requires that we assume a volumetric density of the organic ligands, reasonable errors in the assumed density are not important. For a material with a given electronic structure, the emission of electrons from and the scattering of electrons within the material both scale with the density of the material.[38] Consequently, a calculation using a shell with an assumed density that was lower than the true value would require a corresponding larger thickness to match the experimental data. The net effect is that the variations in density and thickness self-compensate in such a way that the product of the two (which is the number density per unit area) remains essentially identical. Figure 2b illustrates this concept. The two samples depicted in Figure 2b have the same molecular coverage and thus attenuate electrons in a very similar manner. In our calculations, for each molecule we used C atom densities based on the known density of $HS(CH_2)_{11}-(EG)_6-OH$ (1.01 g cm^{-3}) at room temperature. However, we also validated that final ligand densities are not sensitive to modest variations in the assumed density.

To determine the number of ligands per unit area, we calculated the anticipated C/Au XPS intensity ratio for Au nanoparticles of a given diameter with carbon shells of varying thicknesses. Figure 3 shows a typical curve, here for a gold

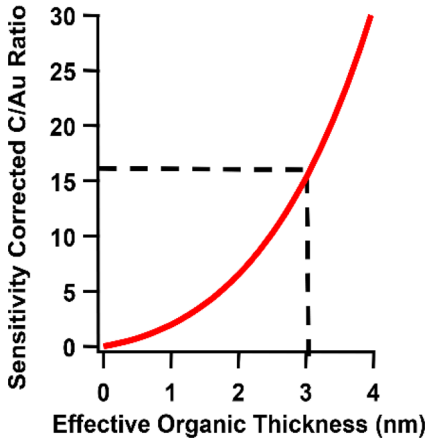

Figure 3. Plot of calculated area ratio A_C/A_{Au} for a 4 nm diameter gold nanoparticle.

nanoparticle 4 nm in diameter. The C/Au ratio that matched the experimental value (here, A_C/A_{Au} = 16.3) thus provides an average thickness of the organic layer (3.1 nm) of the assumed density. Once a C atom density is obtained, division by the number of C atoms per molecule yields the number of molecules per unit area.

Comparison with Experimental Data. Figure 4 shows how the predicted C/Au area ratio varies as a function of particle diameter for organic layers of different discrete thicknesses (here, 1, 2, 3, and 4 nm), as a function of the diameter of the nanoparticle core, along with superimposed experimental measurements for nanoparticles of different core diameters and an experimental data point for a planar sample. For each organic layer thickness, the calculated C/Au area ratio increases rapidly at small core diameters, especially as the organic layer thickness becomes comparable to or even thicker than the diameter of the nanoparticle core.

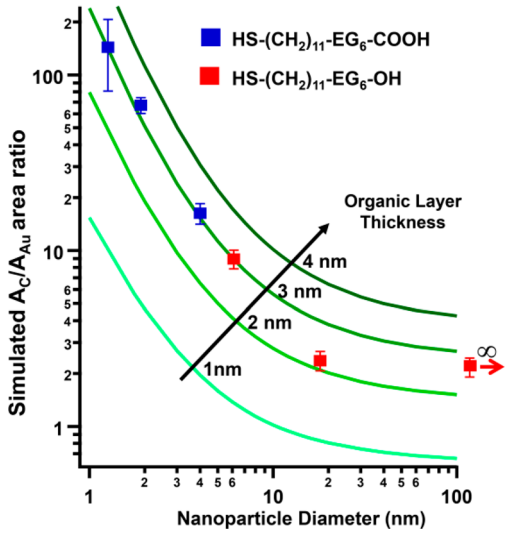

Figure 4. Superimposed experimental data (points) and predicted peak area ratios (curves) A_C/A_{Au} for functionalized Au nanoparticles with different ligand thicknesses. The rightmost data point is from a planar film. The experimental data points fall closely on a line corresponding to a constant effective thickness of 3.0 nm.

In Figure 4, the experimental data for nanoparticles with diameters between 1.3 and 6.1 nm all fall almost exactly on the single line corresponding to a 3 nm organic layer thickness, corresponding to a ligand density of 3.9 molecules nm^{-2}. The data point corresponding to the 18 nm diameter particles lies slightly below this same curve, and is indistinguishable from the planar sample. Notably, the 18 nm diameter sample was synthesized by a different route, and TEM data (see the Supporting Information) show that it is the most heterogeneous in its size distribution. What is more important is that Au nanoparticles in the 1.3–6.1 nm range all yield molecular densities that are identical within the experimental error, even though the XPS A_C/A_{Au} area ratio varies from 8.95 (for 6.1 nm NPs) to 143.8 (for 1.3 nm NPs), representing a factor of 15 difference; moreover, the molecular densities (3.9 ± 0.2 molecules nm^{-2}) are higher than those obtained on a planar surface (3.2 molecules nm^{-2}).

Figure 5 summarizes the apparent enhancement A_C/A_{Au} for organic layers on gold nanoparticles as a function of nanoparticle diameter, for organic layer thicknesses ranging from 1 to 4 nm. These data are normalized relative to what would be observed from a 100 nm diameter particle. For nanoparticles of about 5 nm diameter, the curvature effect leads to enhancements in the A_C/A_{Au} ratio by factors between 3 and 6. Even at 10 nm diameter with a 1 nm layer, the effects are significant and cannot be ignored.

DISCUSSION

The data in Table 1 and in Figure 4 show that the NP films yield a significantly higher A_C/A_{Au} ratio, with the smallest 1.3 nm particles yielding a ratio nearly 80 times the value observed on the planar sample. Analysis of such data without including the proper corrections would vastly overestimate the inferred molecular density. With the numerical evaluation used here, we obtain realistic values that are independent of nanoparticle size. Prior studies have shown that thiolated ligand densities are highest on the Au(111) crystal face, and here the maximum ligand density is 4.6 ligands nm^{-2}.[39] Our data in Figure 4 show

DOI: 10.1021/am507300x
ACS Appl. Mater. Interfaces 2015, 7, 1720–1725

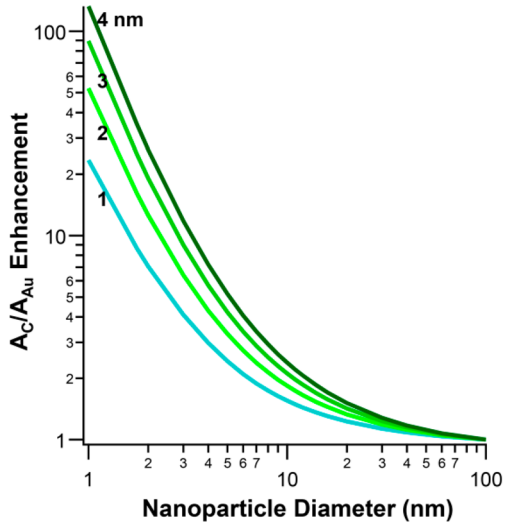

Figure 5. Enhancement A_C/A_{Au} for organic layers on gold nanoparticles as a function of nanoparticle diameter, for organic layer thicknesses ranging from 1 to 4 nm; these data are normalized relative to what would be observed from a 100 nm diameter particle.

that the ligand density is nearly constant for nanoparticles of different diameters, following a line of constant thickness of 3.0 nm, which correlates to a ligand density of 3.9 ± 0.2 molecules nm^{-2}. The data indicate that the ligand density does not change appreciably with nanoparticle diameter. One set of particles (18 nm) is slightly outside of the error bounds established by the other particles. Notably, due to stability problems with such large nanoparticles, the 18 nm diameter particles were prepared by a different route than the other particles, with ligand exchange taking place after formation of the nanoparticle film rather than during initial synthesis. The fact that the 18 nm particles fall slightly below the 3.0 nm thickness line suggests that ligand exchange on these particles may be less complete than on the other particles.

The area density of 3.9 ± 0.2 molecules nm^{-2} we obtain is slightly lower than the expected maximum packing of 4.6 molecules nm^{-2} and near the values of 3.46 molecules nm^{-2} reported previously for $HS(CH_2)_{11}-(EG)_6-OH$ on planar gold.[40] This difference between our value of 3.9 molecules nm^{-2} and the previous value of 3.46 molecules nm^{-2} could arise from the fact that the previous study does not appear to have corrected for scattering of electrons that were generated within the organic layer, thereby underestimating the coverage. Our method properly takes care of scattering in both core and overlayers.

Another important point to observe from Figure 4 is that the nanoparticle diameter where a particle will appear flat is dependent on the nature of a ligand. For example, Hill et. al reported that hybridization of oligo(DNA) oligomers did not resemble a planar surface until nanoparticle diameters approached 60 nm.[8] Following the observed trend, for example, a thick organic layer of 10 nm or greater would need curvature corrections at a deceivingly large size that might otherwise be treated as being planar.

CONCLUSIONS

The above results demonstrate that XPS can be used as a quantitative tool for evaluating ligand densities on nanoparticles even at very small diameters where nanoparticular curvature is important. The influence of electron scattering in the core and in the ligand layer are both included in the model. Small (~1.3 nm) diameter nanoparticles exhibit C/Au ratios more than 15 times those of larger particles and 80 times larger than a flat surface. After applying suitable corrections based on a simple numerical model, our results show that the ligand densities are, within experimental error, identical for all nanoparticle diameters measured. The influence of nanoparticle curvature and the errors introduced using planar-surface models are large for nanoparticles <20 nm diameter and can be significant for larger particles with more extended ligands. The model outlined here can be used with a wide range of core−shell nanoparticles with other types of shells.

ASSOCIATED CONTENT

Supporting Information

Details of nanoparticle synthesis and functionalization. Transmission electron microscopy (TEM) images and size statistics. This material is available free of charge via the Internet at http://pubs.acs.org.

AUTHOR INFORMATION

Corresponding Author

*E-mail: rjhamers@wisc.edu.

Present Addresses

[§]3M Center, Building 0251-02-B-11, Saint Paul, Minnesota 55144-1000, United States.

[∥]The Molecular Foundry, Lawrence Berkeley National Laboratory, Berkeley, California 94720, United States.

[⊥]Department of Chemistry, Physical and Environmental Sciences Program, Colorado Mesa University, 1100 North Avenue, Grand Junction, Colorado 81501, United States.

Notes

The authors declare no competing financial interest.

ACKNOWLEDGMENTS

This work was supported by the National Science Foundation Centers for Chemical Innovation Program, Grant CHE1240151, for the Center for Sustainable Nanotechnology.

ABBREVIATIONS

EAL, electron attenuation length
EG, $-OCH_2CH_2-$ group
EG6, hexaethylene glycol
IMFP, inelastic mean free path
NP, nanoparticle
XPS, X-ray photoelectron spectroscopy

REFERENCES

(1) Baer, D. R.; Engelhard, M. H. XPS Analysis of Nanostructured Materials and Biological Surfaces. *J. Electron Spectrosc. Relat. Phenom.* **2010**, *178−179*, 415−432.

(2) Baer, D. R.; Engelhard, M. H.; Johnson, G. E.; Laskin, J.; Lai, J. F.; Mueller, K.; Munusamy, P.; Thevuthasan, S.; Wang, H. F.; Washton, N.; Elder, A.; Baisch, B. L.; Karakoti, A.; Kuchibhatla, S.; Moon, D. Surface Characterization of Nanomaterials and Nanoparticles: Important Needs and Challenging Opportunities. *J. Vac. Sci. Technol., A* **2013**, *31*, 050820.

(3) Lanterna, A. E.; Coronado, E. A.; Granados, A. M. When Nanoparticle Size and Molecular Geometry Matter: Analyzing the Degree of Surface Functionalization of Gold Nanoparticles with Sulfur Heterocyclic Compounds. *J. Phys. Chem. C* **2012**, *116*, 6520−6529.

DOI: 10.1021/am507300x
ACS Appl. Mater. Interfaces 2015, 7, 1720−1725

(4) Gavia, D. J.; Shon, Y.-S. Controlling Surface Ligand Density and Core Size of Alkanethiolate-Capped Pd Nanoparticles and Their Effects on Catalysis. *Langmuir* **2012**, *28*, 14502−14508.
(5) Becerra, L. R.; Murray, C. B.; Griffin, R. G.; Bawendi, M. G. Investigation of the Surface Morphology of Capped CdSe Nanocrystallites by 31P Nuclear Magnetic Resonance. *J. Chem. Phys.* **1994**, *100*, 3297−3300.
(6) Morris-Cohen, A. J.; Donakowski, M. D.; Knowles, K. E.; Weiss, E. A. The Effect of a Common Purification Procedure on the Chemical Composition of the Surfaces of CdSe Quantum Dots Synthesized with Trioctylphosphine Oxide. *J. Phys. Chem. C* **2009**, *114*, 897−906.
(7) Hinterwirth, H.; Kappel, S.; Waitz, T.; Prohaska, T.; Lindner, W.; Lämmerhofer, M. Quantifying Thiol Ligand Density of Self-Assembled Monolayers on Gold Nanoparticles by Inductively Coupled Plasma−Mass Spectrometry. *ACS Nano* **2013**, *7*, 1129−1136.
(8) Hill, H. D.; Millstone, J. E.; Banholzer, M. J.; Mirkin, C. A. The Role Radius of Curvature Plays in Thiolated Oligonucleotide Loading on Gold Nanoparticles. *ACS Nano* **2009**, *3*, 418−424.
(9) Nanda, J.; Kuruvilla, B. A.; Sarma, D. D. Photoelectron Spectroscopic Study of CdS Nanocrystallites. *Phys. Rev. B* **1999**, *59*, 7473−7479.
(10) Terrasi, A.; Coluzza, C.; Margaritondo, G. Ar^+ Bombardment of Si(100) in Oxygen Atmosphere: Room Temperature Oxide Formation Studied by X-Ray Photoelectron Spectroscopy. *J. Appl. Phys.* **1995**, *78*, 3820−3823.
(11) Williams, J. M.; Beebe, T. P. High-Resolution Algorithm for Quantitative Elemental Depth Profiling by Angle-Resolved X-Ray Photoelectron Spectroscopy. *J. Vac. Sci. Technol., A* **1997**, *15*, 2122−2133.
(12) Nelson, K. E.; Gamble, L.; Jung, L. S.; Boeckl, M. S.; Naeemi, E.; Golledge, S. L.; Sasaki, T.; Castner, D. G.; Campbell, C. T.; Stayton, P. S. Surface Characterization of Mixed Self-Assembled Monolayers Designed for Streptavidin Immobilization. *Langmuir* **2001**, *17*, 2807−2816.
(13) Petrovykh, D. Y.; Kimura-Suda, H.; Whitman, L. J.; Tarlov, M. J. Quantitative Analysis and Characterization of DNA Immobilized on Gold. *J. Am. Chem. Soc.* **2003**, *125*, 5219−5226.
(14) Tosatti, S.; Michel, R.; Textor, M.; Spencer, N. D. Self-Assembled Monolayers of Dodecyl and Hydroxy-Dodecyl Phosphates on Both Smooth and Rough Titanium and Titanium Oxide Surfaces. *Langmuir* **2002**, *18*, 3537−3548.
(15) Pale-Grosdemange, C.; Simon, E. S.; Prime, K. L.; Whitesides, G. M. Formation of Self-Assembled Monolayers by Chemisorption of Derivatives of Oligo(Ethylene Glycol) of Structure HS-$(CH_2)_{11}(OCH_2CH_2)_M$OH on Gold. *J. Am. Chem. Soc.* **1991**, *113*, 12−20.
(16) Laibinis, P. E.; Whitesides, G. M.; Allara, D. L.; Tao, Y. T.; Parikh, A. N.; Nuzzo, R. G. Comparison of the Structures and Wetting Properties of Self-Assembled Monolayers of N-Alkanethiols on the Coinage Metal Surfaces, Copper, Silver, and Gold. *J. Am. Chem. Soc.* **1991**, *113*, 7152−7167.
(17) Herrwerth, S.; Eck, W.; Reinhardt, S.; Grunze, M. Factors That Determine the Protein Resistance of Oligoether Self-Assembled Monolayers - Internal Hydrophilicity, Terminal Hydrophilicity, and Lateral Packing Density. *J. Am. Chem. Soc.* **2003**, *125*, 9359−9366.
(18) Lee, S.; Shon, Y.-S.; Colorado, R.; Guenard, R. L.; Lee, T. R.; Perry, S. S. The Influence of Packing Densities and Surface Order on the Frictional Properties of Alkanethiol Self-Assembled Monolayers (SAMS) on Gold: A Comparison of SAMS Derived from Normal and Spiroalkanedithiols. *Langmuir* **2000**, *16*, 2220−2224.
(19) Snow, A. W.; Jernigan, G. G.; Ancona, M. G. Packing Density of HS(CH2)COOH Self-Assembled Monolayers. *Analyst* **2011**, *136*, 4935−4949.
(20) Sofia, S. J.; Premnath, V.; Merrill, E. W. Poly(Ethylene Oxide) Grafted to Silicon Surfaces: Grafting Density and Protein Adsorption. *Macromolecules* **1998**, *31*, 5059−5070.
(21) Ertl, G.; Küppers, J. *Low-Energy Electrons and Surface Chemistry*; VCH: Weinheim, 1985.
(22) Bain, C. D.; Whitesides, G. M. Attenuation Lengths of Photoelectrons in Hydrocarbon Films. *J. Phys. Chem.* **1989**, *93*, 1670−1673.
(23) Wertheim, G. K.; DiCenzo, S. B. Cluster Growth and Core-Electron Binding Energies in Supported Metal Clusters. *Phys. Rev. B* **1988**, *37*, 844−847.
(24) Tunc, I.; Suzer, S.; Correa-Duarte, M. A.; Liz-Marzán, L. M. XPS Characterization of Au (Core)/SiO2 (Shell) Nanoparticles. *J. Phys. Chem. B* **2005**, *109*, 7597−7600.
(25) Katari, J. E. B.; Colvin, V. L.; Alivisatos, A. P. X-Ray Photoelectron Spectroscopy of CdSe Nanocrystals with Applications to Studies of the Nanocrystal Surface. *J. Phys. Chem.* **1994**, *98*, 4109−4117.
(26) Frydman, A.; Castner, D. G.; Schmal, M.; Campbell, C. T. A Method for Accurate Quantitative XPS Analysis of Multimetallic or Multiphase Catalysts on Support Particles. *J. Catal.* **1995**, *157*, 133−144.
(27) Chatelier, R. C.; St. John, H. A. W.; Gengenbach, T. R.; Kingshott, P.; Griesser, H. J. Incorporation of Surface Topography in the XPS Analysis of Curved or Rough Samples Covered by Thin Multilayers. *Surf. Interface Anal.* **1997**, *25*, 741−746.
(28) Hostetler, M. J.; Murray, R. W. Colloids and Self-Assembled Monolayers. *Curr. Opin. Colloid Interface Sci.* **1997**, *2*, 42−50.
(29) Volkert, A. A.; Subramaniam, V.; Ivanov, M. R.; Goodman, A. M.; Haes, A. J. Salt-Mediated Self-Assembly of Thioctic Acid on Gold Nanoparticles. *ACS Nano* **2011**, *5*, 4570−4580.
(30) Techane, S. D.; Gamble, L. J.; Castner, D. G. Multitechnique Characterization of Self-Assembled Carboxylic Acid-Terminated Alkanethiol Monolayers on Nanoparticle and Flat Gold Surfaces. *J. Phys. Chem. C* **2011**, *115*, 9432−9441.
(31) Shard, A. G.; Wang, J.; Spencer, S. J. XPS Topofactors: Determining Overlayer Thickness on Particles and Fibres. *Surf. Interface Anal.* **2009**, *41*, 541−548.
(32) Techane, S.; Baer, D. R.; Castner, D. G. Simulation and Modeling of Self-Assembled Monolayers of Carboxylic Acid Thiols on Flat and Nanoparticle Gold Surfaces. *Anal. Chem.* **2011**, *83*, 6704−6712.
(33) Harder, P.; Grunze, M.; Dahint, R.; Whitesides, G. M.; Laibinis, P. E. Molecular Conformation in Oligo(Ethylene Glycol)-Terminated Self-Assembled Monolayers on Gold and Silver Surfaces Determines Their Ability to Resist Protein Adsorption. *J. Phys. Chem. B* **1998**, *102*, 426−436.
(34) Lasseter, T. L.; Clare, B. H.; Abbott, N. L.; Hamers, R. J. Covalently Modified Silicon and Diamond Surfaces: Resistance to Nonspecific Protein Adsorption and Optimization for Biosensing. *J. Am. Chem. Soc.* **2004**, *126*, 10220−10221.
(35) Tanuma, S.; Ichimura, S.; Goto, K.; Kimura, T. Experimental Determinations of Electron Inelastic Mean Free Paths in Silver, Gold, Copper and Silicon from Electron Elastic Peak Intensity Ratios. *J. Surf. Anal.* **2002**, *9*, 285−290.
(36) Laibinis, P. E.; Bain, C. D.; Whitesides, G. M. Attenuation of Photoelectrons in Monolayers of N-Alkanethiols Adsorbed on Copper, Silver, and Gold. *J. Phys. Chem.* **1991**, *95*, 7017−7021.
(37) Wagner, C. D. Factors Affecting Quantitative Determinations by X-Ray Photoelectron Spectroscopy. *Anal. Chem.* **1977**, *49*, 1282−1290.
(38) Tanuma, S.; Powell, C. J.; Penn, D. R. Calculations of Electron Inelastic Mean Free Paths. II. Data for 27 Elements over the 50−2000 eV Range. *Surf. Interface Anal.* **1991**, *17*, 911−926.
(39) Schreiber, F. Structure and Growth of Self-Assembling Monolayers. *Prog. Surf. Sci.* **2000**, *65*, 151−257.
(40) Herrwerth, S.; Eck, W.; Reinhardt, S.; Grunze, M. Factors That Determine the Protein Resistance of Oligoether Self-Assembled Monolayers − Internal Hydrophilicity, Terminal Hydrophilicity, and Lateral Packing Density. *J. Am. Chem. Soc.* **2003**, *125*, 9359−9366.

DOI: 10.1021/am507300x
ACS Appl. Mater. Interfaces 2015, 7, 1720−1725